2. Pattern Formation in Reaction-Diffusion Systems

Under the continuum hypothesis, the spatio-temporal state of a chemical system is described by partial differential equations derived from considerations of conservation of matter. We consider the net production rate of a chemical species, the reaction kinetics, within an elemental volume V and the flux of matter through the elemental volume boundary ∂V at fixed location within the reaction space Ω. The reaction space is a bounded region which will be called the *domain*, with boundary $\partial\Omega$. The rate of change of the amount of matter within the elemental volume is given by

$$\frac{\mathrm{d}}{\mathrm{d}t}\int_V c(\mathbf{x},t)\,\mathrm{d}\mathbf{x} = \int_{\partial V} -\mathbf{j}(\mathbf{x},t)\cdot\mathbf{dS} + \int_V R(c,p)\,\mathrm{d}\mathbf{x}, \tag{2.1}$$

where $c(\mathbf{x},t)$ is the concentration of a chemical species C at position $\mathbf{x}$ and time t. The flux $\mathbf{j}(\mathbf{x},t)$ is through the closed surface ∂V and $R(c,p)$ is the net rate of creation of concentration of species C. The reaction kinetics, R, are generally described by a polynomial or rational function in c and p represents interaction with other chemicals and external factors. Using the divergence theorem, (2.1) may be written

$$\frac{\mathrm{d}}{\mathrm{d}t}\int_V c(\mathbf{x},t)\,\mathrm{d}\mathbf{x} = \int_V \left[-\nabla\cdot\mathbf{j} + R(c,p)\right]\mathrm{d}\mathbf{x}. \tag{2.2}$$

The domain is fixed in time and so we may differentiate through the integral. Using the fact that the choice of elemental volume V was arbitrary within Ω, we have that at every point $(\mathbf{x},t)$ the following conservation equation holds

$$\frac{\partial c}{\partial t} = -\nabla\cdot\mathbf{j} + R(c,p). \tag{2.3}$$

If we suppose that the instantaneous flux $\mathbf{j}$ is due to (isotropic) Fickian diffusion then $\mathbf{j} = -D\nabla c$, where the diffusivity D is a constant, and we have the reaction-diffusion equation for species C on a fixed domain Ω

$$\frac{\partial c}{\partial t} = D\nabla^2 c + R(c,p). \tag{2.4}$$

Generally one is interested in the interaction of several chemical species, for example the set $\{C_1, C_2, \ldots, C_n\}$. Equation (2.4) is then replaced by a system of coupled equations which describe the evolution of a vector of concentrations $\mathbf{c} = (c_1, c_2, \ldots, c_n)$, and now $\mathbf{R}(\mathbf{c},p)$ describes the interaction of the species. Various kinetic schemes are presented in Appendix A, and will be introduced in the discussion of the behaviour of specific systems.

2.1 Nondimensionalisation and Boundary Conditions

To nondimensionalise the system of coupled equations we start, following Dillon *et al.* [26], by writing $\bar{c}_i = c_i/\mathcal{C}_i$ and $\bar{\mathbf{x}} = \mathbf{x}/L$. Here L is a length scale (usually taken to be the domain length for problems in one spatial dimension) and $\mathcal{C}_i$ is a reference

concentration for the chemical species C_i. A reaction rate ω, characteristic of the kinetic scheme, is used to nondimensionalise the reaction term which is represented in nondimensional form by $\bar{\mathbf{R}}(\bar{\mathbf{c}}, p)$. In general $\bar{\mathbf{R}}$ has the same functional form as $\mathbf{R}$, but generally has different coefficients.

To standardise the problem (and without loss of generality) we rewrite the system in order of decreasing diffusivity, D_i for the i^{th} species. We introduce a dimensionless scaling parameter

$$\gamma = \frac{\omega L^2}{D_1}, \tag{2.5}$$

where $D_1 = \max\{D_i\}$, which represents the ratio of diffusive T_D to kinetic T_R relaxation times, where

$$T_D = \frac{L^2}{D_1} \quad \text{and} \quad T_R = \frac{1}{\omega}. \tag{2.6}$$

Both of these timescales could be used to nondimensionalise the time variable. For reasons which will become evident later, we choose to nondimensionalise the equations using the kinetic relaxation timescale. Writing $\bar{t} = \omega t$, and dropping the overbars for notational convenience, we have the dimensionless equation

$$\frac{\partial \mathbf{c}}{\partial t} = \frac{1}{\gamma}\mathcal{D}\nabla^2\mathbf{c} + \mathbf{R}(\mathbf{c}, p), \quad \mathbf{x} \in \Omega \tag{2.7}$$

where $\mathcal{D} = \text{diag}[1, d_2, \ldots, d_n]$ is the diagonal matrix containing the ordered dimensionless diffusivities where $d_i = D_i/D_1 \leq 1$ and $d_i \leq d_{i-1}, i = 2, \ldots, n$.

The full specification of the reaction-diffusion system requires that conditions be imposed on the boundary of the solution domain, $\partial\Omega$, and that an initial condition is specified for the system of partial differential equations. If initial data is contained in the vector $\mathbf{c}_0(\mathbf{x})$, then a typical set of boundary conditions is given by

$$(\mathbf{n} \cdot \nabla)\,\mathbf{c} = \mathcal{P}(\mathbf{c}^* - \mathbf{c}), \quad \mathbf{x} \in \partial\Omega \tag{2.8}$$

$$\mathbf{c}(\mathbf{x}, 0) = \mathbf{c}_0(\mathbf{x}) \tag{2.9}$$

where the fixed concentration vector $\mathbf{c}^*$ is uniform over Ω and represents a constant external reference concentration for each species. The outward normal gradient operator $\mathbf{n} \cdot \nabla$ acts component-wise on $\mathbf{c}(\mathbf{x}, t)$, where $\mathbf{n}$ is the outward-pointing vector normal to the boundary. On $\partial\Omega$ we will restrict boundary conditions such that the matrix $\mathcal{P}$ is of the form $\mathcal{P} = \text{diag}[P_1, P_2, \ldots, P_n]$, where constants $0 \leq P_i \leq \infty$ define the type of condition imposed, specifying the rate of flux at the boundary for each species. For *scalar* conditions $\mathcal{P}_{ij} = \delta_{ij}P$ with constant P, where δ_{ij} is the Kronecker delta, and $P = 0$ gives zero flux (Neumann) data for each species while $P = \infty$ corresponds to Dirichlet conditions for which there is an instantaneous equilibrium with the external concentration, $\mathbf{c}^*$. The case for which $\mathbf{c}^* = \mathbf{c}_s$, where

$$\mathbf{R}(\mathbf{c}_s, p) = \mathbf{0} \tag{2.10}$$

is called *homogeneous* Dirichlet conditions. The concentration vector $\mathbf{c}_s$ is the *kinetic steady state* of the reaction scheme, the stability of which we discuss below. Another type of constraint often assumed on $\partial\Omega$ is a periodic boundary condition, taken to simulate a spatially unbounded system. On the one-dimensional domain, for $x \in [0,1]$, periodic conditions take the form $\mathbf{c}(0,t) = \mathbf{c}(1,t)$ for all t.

2.2 Diffusion-Driven Instability

The counterintuitive result of Turing's celebrated paper [126] is that a spatially homogeneous system of interacting chemicals which is stable to perturbation in the absence of diffusion may be driven to a persistent spatially heterogeneous state via a dynamic instability due to diffusion. This statement defines the diffusion-driven (Turing) instability (DDI), which is recognised as one example of a class of pattern forming instabilities in systems driven far from equilibrium. In otherwise similar patterning mechanisms (for example in fluid systems: thermal convection (buoyancy) driving the Rayleigh-Bénard instability or the rotation of concentric cylindrical walls in the Taylor-Couette flow system [21]) the spatial scale of pattern is determined by the geometry of the solution domain (i.e. by physical constraints). Patterns in Turing systems, however, are characterised by a wavelength which is determined by parameters intrinsic to the mechanism of the instability itself, as will be demonstrated in section 2.3.1. In this respect the Turing instability is set apart from other pattern forming systems. For a discussion of the differences between the Turing and Rayleigh-Bénard instabilities in finite systems see Chen and Cross [15]. Next we review the standard results for the onset of the instability in the linear regime (see, for example, Murray [88]), and go on to consider a nonlinear analysis for longer-time behaviour.

2.2.1 Linear Analysis. The defining requirement, stability of the homogeneous (spatially uniform) steady state $\mathbf{c}_s$ to perturbation in the absence of diffusion, is equivalent to requiring that $\mathbf{c}_s$ must be stable to homogeneous perturbations in the presence of the diffusion term. The diffusion-driven instability is the instability of such reaction-diffusion systems to heterogeneous perturbation. Near to onset we study the linear instabilities of the homogeneous steady state to classify the patterns which may grow in terms of their wavenumber (and frequency for spatio-temporal pattern formation).

The homogeneous steady state, positive solution of $\mathbf{R}(\mathbf{c}_s, p) = \mathbf{0}$ with no spatial variation, exists when compatible with the imposed boundary conditions. The analysis is thus restricted to the cases of homogeneous Dirichlet and Neumann (zero flux) conditions. We consider bifurcations from the steady state by examining the response of the system to an initially small perturbation $\mathbf{w}(\mathbf{x},t)$ where $|\mathbf{w}_i(\mathbf{x},0)| \ll 1$. Setting

$$\mathbf{c}(\mathbf{x},t) = \mathbf{c}_s + \mathbf{w}(\mathbf{x},t) \tag{2.11}$$

in the dimensionless reaction-diffusion equation (2.7) we linearise in the variable $\mathbf{w}$ giving

$$\frac{\partial \mathbf{w}}{\partial t} = \frac{1}{\gamma}\mathcal{D}\nabla^2\mathbf{w} + \mathcal{A}\mathbf{w} \tag{2.12}$$

where the Jacobian (stability) matrix $\mathcal{A}$ is evaluated at the homogeneous steady state

$$\mathcal{A}_{ij} = \left.\frac{\partial R_i}{\partial c_j}\right|_{c_s}. \tag{2.13}$$

We consider scalar boundary conditions

$$(\mathbf{n}\cdot\nabla)\,\mathbf{w} = -P\mathbf{w} \quad \text{on } \partial\Omega, \tag{2.14}$$

restricting ourselves to the homogeneous case, $\mathbf{c}^* = \mathbf{c}_s$. Solutions of system (2.12)–(2.14) take the general form $\mathbf{w}(\mathbf{x},t) = \exp(\lambda t)\,\Phi(\mathbf{x})$ where Φ is a vector and the growth rate may be complex, $\lambda = \alpha + i\beta$, allowing for temporal oscillation. Substituting this solution into equation (2.12) we obtain

$$\frac{1}{\gamma}\mathcal{D}\nabla^2\Phi + (\mathcal{A} - \lambda\mathcal{I})\Phi = 0 \tag{2.15}$$

where $\mathcal{I}$ is the identity.

Eigenfunctions of the spatial eigenvalue problem (2.15) can be written as $\Phi_m = \mathbf{y}_m\phi_m$, where $\mathbf{y}_m$ is a constant vector and $\phi_m(\mathbf{x})$ are (scalar) eigenfunctions of the Laplacian containing the spatial dependency of the solution, and are subject to the scalar boundary conditions

$$\begin{aligned} \nabla^2\phi_m &= -k_m^2\phi_m \quad \text{in } \Omega \\ \mathbf{n}\cdot\nabla\phi_m &= -P\phi_m \quad \text{on } \partial\Omega, \end{aligned} \tag{2.16}$$

where k_m is a dimensionless wavenumber associated with ϕ_m. The boundary conditions acting on Φ restrict the spatial dependency to a discrete set of eigenfunctions of the Laplacian, ϕ_m. Clearly, for the solution on an unbounded domain, the wavenumber k is a continuous variable. For nontrivial solutions of (2.15) we require

$$\det\left[\mathcal{A} - \frac{k_m^2}{\gamma}\mathcal{D} - \lambda(k_m^2)\mathcal{I}\right] = 0 \tag{2.17}$$

(the characteristic polynomial) which yields the *dispersion relation*, $\lambda = \lambda(k_m^2)$, an algebraic equation for the growth rate. The solution of the linear stability problem is then given by

$$\mathbf{w}(\mathbf{x},t) = \sum_{m=0}^{\infty} \exp\left(\lambda(k_m^2)t\right)\mathbf{y}_m\phi_m(\mathbf{x}) \tag{2.18}$$

where the vector $\mathbf{y}_m$ is determined by the initial data $\mathbf{w}_0(\mathbf{x}) = \mathbf{c}_0(\mathbf{x}) - \mathbf{c}_s$. The individual components making up the infinite sum (2.18) are *linear modes* and the label m is the relevant *mode number*. For certain nonlinearities in the reaction term

the amplitudes of growing modes are bounded to finite value. This is shown in the nonlinear analysis below. We distinguish between the eigenfunctions of the Laplacian (the linear modes) and the patterns which subsequently develop outside the linear regime, which we will call *pattern modes*.

The linear stability of the homogeneous steady state to spatially heterogeneous perturbation of mode m is determined by the sign of the real part of $\lambda(k_m^2)$. The kinetic steady state has neutral stability for $\mathcal{R}e\,\lambda = 0$, is (asymptotically) stable for $\mathcal{R}e\,\lambda < 0$ and is unstable (and hence a perturbing mode of appropriate wavenumber may grow) for $\mathcal{R}e\,\lambda > 0$. This latter possibility describes the onset of the diffusion-driven instability. We describe any mode for which the linear stability analysis predicts instability of the homogeneous steady state as a *growing* mode. Depending on the components of $\mathbf{y}_m$, determined by the initial conditions, all possible modes may not be available for growth. The question of which mode grows to become the final long term pattern, the *pattern selection* problem, will be discussed later. The requirement that the steady state is stable in the absence of diffusion is equivalent to there being no growing mode with wavenumber $k_0 = 0$, that is, $\mathcal{R}e\,\lambda(k_0 = 0) < 0$. This provides certain conditions on the components of the Jacobian matrix, $\mathcal{A}$, as will be demonstrated explicitly from the linear analysis in the simple case of a two-component reaction-diffusion system in one spatial dimension.

2.2.2 Two-Component Model System. We consider a reaction-diffusion model of two interacting species $\mathbf{c} = (u, v)$ in one spatial dimension, with external reference concentrations set at the homogeneous steady state of the kinetics, $\mathbf{R}(\mathbf{c}_s, p) = \big(f(u_s, v_s), g(u_s, v_s)\big) = \mathbf{0}$, and scalar boundary conditions. Linearising about the steady state and writing $\mathbf{w} = \mathbf{c} - \mathbf{c}_s$ we have

$$\frac{\partial \mathbf{w}}{\partial t} = \frac{1}{\gamma}\mathcal{D}\frac{\partial^2 \mathbf{w}}{\partial x^2} + \mathcal{A}\mathbf{w}, \quad x \in [0,1] \tag{2.19}$$

$$\frac{\partial \mathbf{w}}{\partial x} = P\mathbf{w}, \qquad\qquad x = 0, 1 \tag{2.20}$$

with

$$\mathcal{A} = \left[\begin{array}{cc} f_u & f_v \\ g_u & g_v \end{array}\right]_{(u_s, v_s)} \quad \text{and} \quad \mathcal{D} = \left[\begin{array}{cc} 1 & 0 \\ 0 & d \end{array}\right]. \tag{2.21}$$

Henceforth, the partial derivatives f_u, f_v, g_u and g_v will be assumed to be evaluated at the steady state (u_s, v_s). From (2.17) we have $\det\left(\mathcal{A} - k_m^2\mathcal{D}/\gamma - \lambda(k_m^2)\mathcal{I}\right) = 0$, which yields the dispersion relation for this problem

$$0 = \lambda^2 + \lambda\left(\frac{k_m^2}{\gamma}(1+d) - (f_u + g_v)\right) + h(k_m^2), \tag{2.22}$$

where

$$h(k_m^2) = \frac{d}{\gamma^2}k_m^4 - \frac{1}{\gamma}\left(df_u + g_v\right)k_m^2 + f_u g_v - f_v g_u. \tag{2.23}$$

Firstly, let us address the requirement of linear stability in the absence of diffusion. Substituting $k_m = 0$, in the absence of diffusion (or for homogeneous perturbation), into equations (2.22) and (2.23) we have $\lambda_{0,\pm}$ are the roots of

$$\lambda^2 - \lambda(f_u + g_v) + f_u g_v - f_v g_u = 0 \tag{2.24}$$

and so linear stability, $\mathcal{R}e\,\lambda_{0,\pm} < 0$, is guaranteed by the two constraints

$$\mathrm{tr}\mathcal{A} = f_u + g_v < 0, \quad \det\mathcal{A} = f_u g_v - f_v g_u > 0. \tag{2.25}$$

Next we consider spatially heterogeneous perturbations for which $k_m \neq 0$. In order to achieve the growth of some linear mode we require that there is at least one real k_m for which $\mathcal{R}e\,\lambda > 0$. From the dispersion relation we see that the first requirement of (2.25) precludes the coefficient of λ from taking a negative value, and so we must have $h(k_m^2) < 0$ for diffusion-driven instability. The second of (2.25) implies that this can only be the case if

$$df_u + g_v > 0, \tag{2.26}$$

which provides a third constraint on the system. Comparing with the first of (2.25), this implies that $d \neq 1$, which provides a necessary but not sufficient condition to ensure $\mathcal{R}e\,\lambda > 0$. The criterion for $h(k_m^2)$ to be negative, found by examining the minimum of the function, h_{min}, provides a fourth constraint for diffusion-driven instability,

$$h_{min} = \det\mathcal{A} - \frac{1}{4d}\left(df_u + g_v\right)^2 < 0. \tag{2.27}$$

Collecting together the four conditions that we have computed and which must be satisfied for the Turing instability we have:

- $f_u + g_v < 0$
- $f_u g_v - f_v g_u > 0$
- $df_u + g_v > 0$
- $f_u g_v - f_v g_u - \frac{1}{4d}\left(df_u + g_v\right)^2 < 0$

where the partial derivatives are evaluated at the kinetic steady state.

These four conditions may be employed to deduce parameter regimes for which specific kinetic schemes can undergo Turing bifurcation, or indeed whether such a bifurcation is possible for a particular reaction scheme. The region of the parameter space for a particular kinetic scheme within which the diffusion-driven instability may give rise to pattern is known as the *Turing space* [88]. For anything but the simplest form for $\mathbf{R}$ and hence $\mathcal{A}$ in (2.13), the direct algebraic calculation of the boundaries of the Turing space (given by the above conditions) is intractable. Murray [87] has described a parametric approach by which the problem is considerably simplified. The existence of a Turing space does not in itself guarantee that a pattern will arise from the dynamic instability in a *finite* system, where only a discrete set of linear modes is

consistent with the domain geometry and boundary conditions, at least one of which must have positive linear growth rate. This is discussed further in section 2.2.4

2.2.3 Configurations of the Jacobian. The two constraints (2.25), derived for the stability of homogeneous perturbations, lead to a restriction on the configuration of the signs of components for the Jacobian matrix $\mathcal{A}$. With $d \leq 1$, the constraints $f_u + g_v < 0$ and $df_u + g_v > 0$ require that $f_u < 0$ and $g_v > 0$, and $\det \mathcal{A} > 0$ implies that only the following configurations are compatible with diffusion-driven instability

$$\mathrm{sgn}(\mathcal{A}_p) \equiv \begin{bmatrix} - & + \\ - & + \end{bmatrix}, \quad \mathrm{sgn}(\mathcal{A}_c) \equiv \begin{bmatrix} - & - \\ + & + \end{bmatrix}. \tag{2.28}$$

The first of these is called a *pure* and the second a *cross activator-inhibitor* mechanism. The interpretation of these two possibilities in terms of activation and inhibition may be gleaned from an examination of the nullclines of systems with Jacobian matrix of these general forms. A pure system is one in which v is self-activating and also activates u, while u reciprocally inhibits v and is self-inhibiting. On the other hand, for a cross system v is self-activating but inhibits u, while u is still self-inhibiting, but now activates v. In both cases u is deemed to be the (self-) *inhibitor* and v the (self-) *activator*,[1] and with $d \leq 1$ the inhibitor diffuses faster than the activator.[2] This leads to the popular description [98, 88] of the mechanism as one of short range *local* activation with long range *lateral* inhibition. The constraint $\mathrm{tr}\mathcal{A} < 0$ implies that the self-inhibition is always stronger than the self-activation in reaction-diffusion systems of this type that are capable of forming pattern.

One important consequence of these sign configurations, and a feature distinguishing the two cases, is the relative polarity, or phase, of the patterns formed in the systems. Dillon *et al.* [26] show analytically that if the kinetic terms of a two-component reaction-diffusion system in one spatial dimension with zero flux boundary conditions are of the pure variety, then near to a primary bifurcation point the spatial gradients of the species' concentrations will be of the same sign (spatial oscillation in phase) at all points in the domain. For kinetics that are cross-type, the gradients are of opposite sign (spatial oscillation in antiphase) [111]. This result, it is conjectured, is maintained on primary bifurcating solutions away from the bifurcation point.

2.2.4 The Dispersion Relation. The quadratic form of the dispersion relation dictates that the values of k^2 for which the real part of $\lambda(k^2)$ is positive lie in a bounded range $k_-^2 < k^2 < k_+^2$ (of growing modes), given by the zeros of $h(k^2)$,

$$\frac{2d}{\gamma} k_\pm^2 \;=\; (df_u + g_v) \pm \sqrt{(df_u + g_v)^2 - 4d \,\det \mathcal{A}} \;=\; A \pm B \tag{2.29}$$

[1] Some authors reserve the term *activator-inhibitor* to refer to pure kinetics and call cross systems, where the (self-) inhibitor promotes the activator species, *activator-substrate* kinetics.

[2] If we had chosen the opposite ordering for the species, giving $d_i \geq 1$ and prompting $f_u > 0$, this would swap the roles of u and v, amounting only to a relabelling of the two species.

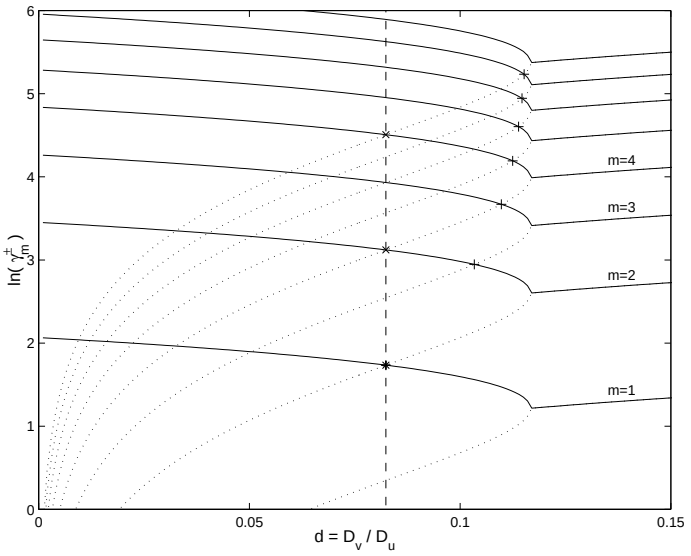

FIGURE 2.1 Intervals of instability of the homogeneous steady state to perturbation by spatial eigenfunctions of the Laplacian for Schnakenberg kinetics. We plot the natural logarithms of $\gamma_m^+(d)$ (solid) and $\gamma_m^-(d)$ (dotted) against the ratio of diffusivities d for modes $m = 1, \ldots, 8$, where $k_m = m\pi$. Points for which $\gamma_m^+ = \gamma_{m+1}^-$ are marked + and points where $\gamma_{m_n}^+ = \gamma_{m_{n+1}}^-$ where $m_n = m_0 2^n$ are marked by $\times$, which lie on a line of equal d (dashed). Note that for successively smaller d there is increasing overlap between the ranges of instability for different modes. The curves are calculated for Schnakenberg kinetics (see Appendix A.1) with kinetic parameters $a = 0.1$ and $b = 0.9$. Note that the bifurcation occurs at the same value $d = d_c$ independent of m (the bifurcation point is in fact independent of k - see equation (2.34).

where A and B depend on the kinetic parameters and d but not on γ.[3] For fixed kinetic parameters p this condition is satisfied when the scaling parameter falls in the interval $\gamma \in [\gamma_m^-, \gamma_m^+]$, where, making the dependence on d explicit,

$$\gamma_m^-(d) = \frac{2dk_m^2}{A(d) + B(d)} \quad \text{and} \quad \gamma_m^+(d) = \frac{2dk_m^2}{A(d) - B(d)}. \tag{2.30}$$

Successive ranges of instability overlap when $\gamma_m^+ > \gamma_{m+1}^-$ and there is an interval of stability of the homogeneous steady state when $\gamma_m^+ < \gamma_{m+1}^-$. For zero flux boundary conditions the spatial eigenfunctions are $\phi_m(x) = \cos(m\pi x)$. The instability intervals for $k_m = m\pi$ are plotted for a particular kinetic scheme in Figure 2.1 as d varies. In this case we have overlapping instability ranges (and intervals of stability) for, respectively,

$$1 + \frac{2m^2}{2m+1} \quad \geq \frac{A}{B} \quad \left(< \frac{A}{B} \right). \tag{2.31}$$

Points where the equality holds, that is where successive modes first become destabilising at the same value of d, are marked by '+'. We also indicate points at which

[3] For solutions on a bounded domain we also require that there is at least one discrete wavenumber k_m in the range of instability.

destabilising linear patterns of mode $m = m_0 2^n$ and $m = m_0 2^{n+1}$ first coincide, marked by '$\times$', and from (2.30) it can be shown that for $k_m = m\pi$ the corresponding value of d is independent of m_0 and n, shown by the dashed line in the figure. We discuss this result further later in this chapter.

When the ranges of instability for two or more wavenumbers overlap, there is competition between patterning modes. It is apparent from Figure 2.1 that there is increasing overlap further away from the bifurcation point (for example, as d decreases), and intervals of stability tend to disappear. The prediction from linear analysis that the mode with fastest linear growth rate, $\max_m \{\lambda(k_m^2)\}$, will be established proves to be of decreasing validity further from the bifurcation point, and of little use for problems in more than one spatial dimension where there is also increasing degeneracy for pattern orientation. The mechanism of pattern selection, by which one mode is chosen to grow to heterogeneous steady state from many admissible modes, is an important issue to which we will return later in this chapter.

Notably the linear solutions for zero flux conditions have an arbitrary phase shift of π, that is, the linear modes may be reflected about the homogeneous state and remain valid solutions. In fact linear solutions for any boundary conditions or geometry (or spatial dimension) have an arbitrary sign to the wavevector (only the magnitude is determined by the analysis). Thus for zero flux conditions patterns of the same spatial mode number may take one of two polarities, where we adopt the notation that mode $+m$, has positive polarity (high amplitude at the left-hand boundary) and mode $-m$ is of negative polarity. We also recall that pure kinetics will give the same polarity for both species while for cross kinetics the polarities will be opposites.

2.3 Instability and Characteristic Scales

By allowing λ to be complex in the previous analysis we admit the possibility of temporal or spatial oscillation, or both simultaneously. Following Cross and Hohenberg [21] we may in general characterise pattern-forming instabilities at the bifurcation point. For $\lambda = \alpha + i\beta$ and wavenumber k_c at this critical point, where $\alpha = 0$, instability is categorised according to which of k_c and β are non-zero:

1. $k_c \neq 0$ and $\beta = 0$: Spatial oscillation only. Long-time solutions are stationary and spatially heterogeneous structures.
2. $k_c = 0$ and $\beta \neq 0$: Temporal-oscillation only. At large times solutions remain spatially homogeneous.
3. $k_c \neq 0$ and $\beta \neq 0$: Spatio-temporal patterns. Long-time behaviour continues to evolve spatially and temporally.

General instabilities in systems driven far from equilibrium may be of any of the above types. The Turing bifurcation may give rise to instabilities of type (1) and (3). Type (2), corresponding to Hopf bifurcation in the kinetics, is excluded by the requirement that the homogeneous state is stable in the absence of diffusion. For the case of

two species interaction, the dispersion relation subject to the constraints for diffusion-driven instability precludes time-oscillating pattern solutions. We see from (2.22)–(2.23) that λ has an imaginary part when

$$\left(\frac{k_m^2}{\gamma}(1+d)-(f_u+g_v)\right)^2 - 4h(k_m^2) < 0. \tag{2.32}$$

However, for the homogeneous steady state to be unstable to heterogeneous perturbation (for a particular mode to grow to a heterogeneous pattern) we require that $h(k_m^2) < 0$. Hence, for any growing mode, λ must be purely real and so time-oscillatory diffusion-driven instability is not possible in a two-component system of this form. For three or more interacting species, however, the dispersion relation does in general admit such solutions, and we investigate a specific example with three species in Chapter 4.

At a primary bifurcation point the critical wavenumber is defined to be the wavenumber at which the dispersion relation first crosses the axis into the positive half-plane. A critical (maximum) value for the ratio of diffusivities is also determined at this point (see Figure 2.1). We may also recover a characteristic spatial scale from the critical wavelength, and a timescale from the growth rates predicted by the linear analysis.

In section 2.2.4 we have shown that the scaling parameter must lie in a given interval, $\gamma \in [\gamma_m^-, \gamma_m^+]$, for a particular linear mode m to grow. If we consider increasing γ from just greater than zero (there is a singular point where $\gamma = 0$) then we may define a critical value γ_c at which the homogeneous steady state first loses stability to a growing mode, the lowest mode available to the system. For γ below this value no pattern is possible. Hence for pattern we require

$$\gamma > \gamma_c = \gamma_{m_l}^- \tag{2.33}$$

where m_l labels the lowest mode. For the Neumann problem, in the absence of any reaction terms we have relaxation to an average homogeneous concentration vector, the value of which is set by the initial conditions. We might expect the system to relax to such a steady state whenever the relaxation time for diffusion is much smaller than the characteristic timescale of the kinetics. Indeed this intuition is borne out by the minimum requirement on γ. As pointed out by Arcuri and Murray [3], this condition may be interpreted in three ways:

1. $1/\gamma$ is proportional to the largest of the diffusivities, D_1, which must therefore be smaller than some threshold value.
2. The characteristic reaction rate for the kinetics, ω, which is proportional to γ, must be greater than a minimum reaction speed.
3. There is a minimum domain length, proportional to $\sqrt{\gamma_c}$.

Given that γ represents the relative strengths of the reaction and diffusion mechanisms, all of these conditions are equivalent. However, in the context of pattern formation on growing domains the last of these interpretations is the most relevant.

At the bifurcation point the critical wavenumber is determined by equation (2.29) when $k_c = k_+ = k_-$. Thus we must have $B(d) = 0$ which occurs at the critical diffusivity, $d = d_c$, given by the appropriate root, for $0 \leq d_c < 1$, of

$$d = d_\pm = \frac{\det \mathcal{A} - f_v g_u \pm 2\sqrt{-f_v g_u \det \mathcal{A}}}{f_u^2} \tag{2.34}$$

which is independent of k and γ. This imposes a maximum (fractional) value for d, the ratio of diffusivities, where we require $0 \leq d < d_c$ for diffusion-driven instability. However, as has been pointed out in the literature [51, 110, 26], for certain kinetic schemes the critical ratio of diffusivities may be arbitrarily close to unity.

2.3.1 A Spatial Scale: Critical Wavenumber k_c. At the bifurcation point the critical wavenumber is given by

$$k_c = \sqrt{\frac{\gamma(d_c f_u + g_v)}{2d_c}}, \tag{2.35}$$

from which we see that k_c varies as $\sqrt{\gamma}$. Therefore the corresponding dimensional critical wavenumber is independent of the domain length and constitutes a characteristic scale, intrinsic to the system. Turing defined the related wavelength, the *chemical wavelength*, at marginal instability. For a finite bounded system, the critical wavenumber may be defined as the closest admissible wavenumber to k_c.

2.3.2 A Temporal Scale: Maximum Growth Rate λ_{max}. From the dispersion relation we can show that the linear prediction for the maximum growth rate λ_{max} is independent of the scaling parameter γ. We note that the occurrence of γ in equations (2.22)–(2.23) is such that we may consider $\lambda = \lambda(k^2/\gamma)$ with γ appearing nowhere else explicitly. Thus the curve $\lambda(k^2, \gamma)$ as a function of γ for different k is simply scaled along the γ axis, and the maximum value of the function does not change (see Figure 2.2). Hence λ_{max} is a function only of the kinetic parameters and the ratio of diffusivities and we may take $T_\lambda = 1/\lambda_{max}$ to define a characteristic timescale for pattern development. The reaction-diffusion equation was nondimensionalised to have a unit timescale for reaction, hence we expect $T_\lambda \sim \mathcal{O}(1)$. In Table 2.1, values of T_λ (and equivalently, growth rates λ_{max}) calculated for different d for Schnakenberg kinetics are presented, showing that the timescale for pattern formation is reduced as d decreases from d_c. This timescale is intrinsic to the linearised equations and thus to the initial time evolution of the solution, while being independent of the scaling parameter.

d	0.1	0.05	0.01
λ_{max}	0.0572	0.263	0.547
T_λ	17.50	3.80	1.83

TABLE 2.1 Timescale for linear pattern growth $T_\lambda = 1/\lambda_{max}$ (in nondimensional units) for different values of d, the ratio of diffusivities, calculated from the dispersion relation for Schnakenberg kinetics (illustrated in Figure 2.2). Equivalently, λ_{max} represents a pattern growth *rate*.

2.4 Nonlinear Bifurcation Analysis

As we have shown, linear stability theory serves to analyse the response of the homogeneous steady state of a dissipative system to infinitesimal perturbations, allowing determination of the critical conditions for the onset of instability. Turing considered reaction-diffusion equations with linear kinetics. In his paper he sidesteps the issue of unbounded exponential growth by proposing that any such linear model is only applicable to the initial stages of patterning of a real chemical system, and that bounded steady amplitude will be achieved outside the range of applicability of the model. However, nonlinear terms in realistic kinetic schemes can be shown to bound the solution to finite values.

The analytical investigation of instabilities usually proceeds by identifying a control parameter in the system (here, for example, one of the kinetic parameters, the ratio of diffusion coefficients, d, or the scaling parameter, γ) which may be varied until the homogeneous steady state loses stability to a particular heterogeneous solution. The exchange of stability occurs at the bifurcation point, where the curve $\mathcal{R}e\,\lambda$ first moves into the positive half-plane. Close to bifurcation the structure of the long-time solutions may be determined by a nonlinear bifurcation analysis, which we describe here. Such analyses are described as *weakly nonlinear* as the perturbation procedure operates about the critical point of linear stability theory [133]. The method considers *primary* bifurcation branches: nontrivial solutions which bifurcate from the homogeneous steady state (the location of which does not depend on the bifurcation parameter). The approach that we take follows the discussion in the book by Grindrod [46] (see also [93, 5]).

2.4.1 Multiscale Expansion Method. We choose the ratio of diffusivities, d, as the bifurcation parameter and we wish to examine the dependence of solutions on γ. From section 2.3 we see that bifurcation to a spatially heterogeneous state occurs when d passes through the critical value $d = d_c$. As d decreases through d_c we anticipate a pitchfork-type bifurcation for the state variable $\mathbf{c}(x,t)$, with the homogeneous steady state $\mathbf{c}_s$ losing stability to two bifurcating branches corresponding to the two polarities available to the heterogeneous solution.

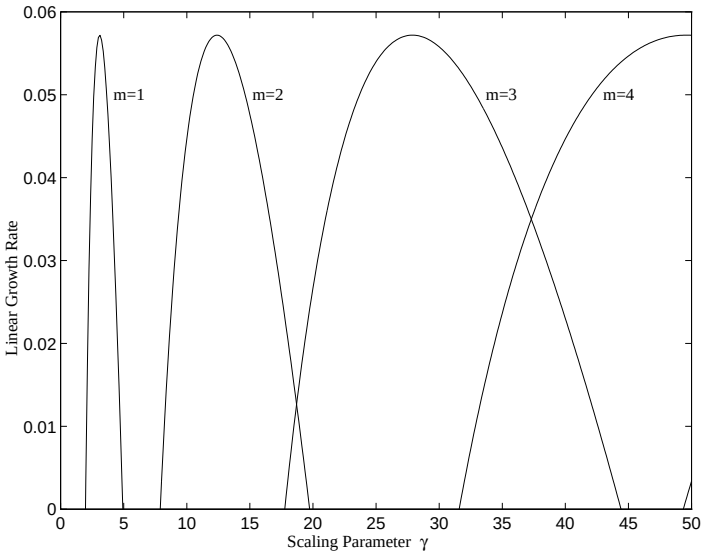

FIGURE 2.2 Real part of linear growth rate λ plotted as a function of scaling parameter γ for the first four linear modes, showing that the maximum growth rate is independent of mode m, where $k_m = m\pi$. We use Schnakenberg kinetics, with $a = 0.1$, $b = 0.9$ and ratio of diffusivities $d = 0.1$ such that an interval of stability is observed for $\gamma \in [5, 8]$.

The time evolution of the bifurcating solutions may be investigated by introducing a small parameter ϵ, where $0 < \epsilon \ll 1$. We set $d_c - d = \epsilon^2$ so that the system lies just inside the region of linear instability and then consider a multiscale expansion in time. Generally the control parameter d is expanded as a series in increasing powers of ϵ, but here we anticipate the pitchfork form for the bifurcation for which the second power is the natural choice. However, the analysis would seek out this expansion had the leading power been initially undetermined.

The Taylor expansion of $\lambda(k^2, d)$ about d_c gives

$$\lambda(d) = \lambda(d_c) - \epsilon^2 \frac{\partial \lambda}{\partial d}\bigg|_{d=d_c} + \mathcal{O}(\epsilon^4) \tag{2.36}$$

with λ a decreasing function of d. The first term on the right-hand side vanishes by the definition of the bifurcation point, giving linear growth $\exp(\lambda t) \sim \exp\left(\mathcal{O}\left(\epsilon^2\right) t\right)$. This suggests that there are three timescales for pattern formation in the static problem:

- $t = \mathcal{O}(1)$: the linear regime in which small amplitude linear modes grow from initial data,
- $t = \mathcal{O}(1/\epsilon^2)$: the nonlinear regime in which the modes interact through the nonlinearities, and
- $t \to \infty$: in which the long-time steady state pattern is achieved.

To investigate the nonlinear regime we introduce the long timescale $\tau = \epsilon^2 t$, and assume that t and τ are independent variables. Then $\partial \mathbf{c}/\partial t$ becomes $\partial \mathbf{c}/\partial t + \epsilon^2 \partial \mathbf{c}/\partial \tau$. Again, in the most general case, we could include a series of timescales, $t = t_0 + \epsilon t_1 +$

$\epsilon^2 t_2 + \ldots + \epsilon^n t_n + \ldots$, and determine which of those were relevant to the problem in the course of the analysis.

Confinement to the finite domain allows the system under investigation to be categorised as one of *small spatial extent*, i.e. the product $Lk \sim \mathcal{O}(1)$. The spectrum of allowed wavenumbers, k_m, is discrete and so for d close to d_c we may consider that only one mode (or a small number of modes at worst) will destabilise the homogeneous state. We will assume that the region of the dispersion relation for which $\mathcal{R}e\,\lambda > 0$ contains only one admissible mode. Therefore we suppose that the corresponding spatial eigenfunction $\phi_m(x)$ determines the spatial dependence in the dominant part of the solution in the nonlinear regime. For systems of large or infinite spatial extent one must consider initially undetermined spatial scalings which results in an envelope-type modulation of the spatial dependency through a *phase* equation [93]. We will assume that pattern evolution in the nonlinear regime is over the timescale of τ (so that we can consider t and τ to be independent) and seek solutions of the form

$$\mathbf{c} = \mathbf{c}_0 + \sum_{n=1}^{\infty} \epsilon^n \mathbf{c}_n(x, t, \tau) \tag{2.37}$$

for which the $\mathbf{c}_n = (u_n, v_n) \sim \mathcal{O}(1)$ are orthogonal. We expand the kinetic terms $\mathbf{R}(\mathbf{c}, p)$ as a Taylor series and, on rearranging, find that the $\mathcal{O}(1)$ solution (the homogeneous solution $\mathbf{c}_0 = \mathbf{c}_s$) drops out of both sides of the equation. We are left with linear equations in (u_n, v_n) for each order of ϵ^n

$$\mathcal{L} \cdot \begin{pmatrix} u_n \\ v_n \end{pmatrix} = \mathcal{Q}_n \tag{2.38}$$

in which $\mathcal{L}$ is the linear differential operator defined by

$$\mathcal{L} = \mathcal{I}\frac{\partial}{\partial t} - \frac{1}{\gamma}\mathcal{D}_c \frac{\partial^2}{\partial x^2} - \mathcal{A} \tag{2.39}$$

where $\mathcal{A}$ is the stability matrix given by equation (2.13) and contains the linear terms from the Taylor expansion of $\mathbf{R}$, and $\mathcal{D}_c = \mathrm{diag}[1, d_c]$. The $\mathcal{Q}_n$ contain the higher order (nonlinear) terms from $\mathbf{R}$ and the remaining terms from the expansion:

$$\mathcal{Q}_1 = \mathbf{0} \tag{2.40}$$

$$\mathcal{Q}_2 = \frac{1}{2}u_1^2 \mathbf{R}_{uu} + u_1 v_1 \mathbf{R}_{uv} + \frac{1}{2}v_1^2 \mathbf{R}_{vv} \tag{2.41}$$

$$\begin{aligned} \mathcal{Q}_3 = &- \begin{pmatrix} 0 \\ 1 \end{pmatrix} \frac{1}{\gamma}\frac{\partial^2 v_1}{\partial x^2} - \frac{\partial \mathbf{c}_1}{\partial \tau} \\ &+ u_1 u_2 \mathbf{R}_{uu} + (u_1 v_2 + u_2 v_1)\mathbf{R}_{uv} + v_1 v_2 \mathbf{R}_{vv} \\ &+ \frac{1}{6}u_1^3 \mathbf{R}_{uuu} + \frac{1}{2}u_1^2 v_1 \mathbf{R}_{uuv} + \frac{1}{2}u_1 v_1^2 \mathbf{R}_{uvv} + \frac{1}{6}v_1^3 \mathbf{R}_{vvv} \end{aligned} \tag{2.42}$$

$$\mathcal{Q}_4 = \ldots$$

where $\mathbf{R}_{uu}, \mathbf{R}_{uv}, \ldots$ denote component-wise partial differentiation of the reaction vector field $\mathbf{R}(\mathbf{c}, p)$ evaluated at the kinetic steady state $\mathbf{c}_s = (u_s, v_s)$. Such terms are functions of $(\mathbf{c}_s, p)$ only, and many of these terms will in fact be zero, for a particular kinetic scheme.

At $\mathcal{O}(\epsilon)$ we recover the linear approximation for the chosen boundary conditions, which is given by

$$\left[\mathcal{I}\frac{\partial}{\partial t} - \frac{1}{\gamma}\mathcal{D}_c\frac{\partial^2}{\partial x^2} - \mathcal{A}\right]\mathbf{c}_1 = \mathbf{0}. \tag{2.43}$$

Considering the linear analysis above, we have that the general solution of this equation takes the form

$$\mathbf{c}_1(x,t,\tau) = \sum_{m=0}^{\infty} \mathbf{a}_m(\tau)\ \exp(\lambda_m t)\cos(k_m x)\,. \tag{2.44}$$

However, the condition of small spatial extent allows us to neglect all k_m except the destabilising mode, k_f say. The functions $\mathbf{a}_m(\tau)$ contain the dependence on the slow time τ. As t becomes large and for $\lambda(k_f^2) \sim 0$ for $d \sim d_c$, the solution to equation (2.43) becomes

$$\mathbf{c}_1(x,\tau) = a(\tau)\begin{pmatrix} \bar{u} \\ \bar{v} \end{pmatrix}\cos(k_f x) \tag{2.45}$$

where $\bar{\mathbf{c}} = (\bar{u}, \bar{v})$ is the nullvector, and $\lambda(k_f^2)$ the relevant eigenvalue, of the matrix

$$\mathcal{A} - \frac{k_f^2}{\gamma}\mathcal{D}_c. \tag{2.46}$$

The signs of $\bar{u}$ and $\bar{v}$ are the same for pure kinetics and are opposite for cross kinetics, consistent with the concentration profile polarities in the two cases. The solution amplitude to first order, $a(\tau)$, is yet to be determined in the analysis.

At $\mathcal{O}(\epsilon^2)$, after substituting the expressions calculated for u_1 and v_1, the components of $\mathcal{Q}_2$ will contain terms with spatial dependence $\cos^2(k_f x)$. The Fredholm Alternative Theorem [60] guarantees the existence and uniqueness of solutions of the linear equation $\mathcal{L}\mathbf{c}_2 = \mathcal{Q}_2$ if the vector $\mathcal{Q}_2$ is orthogonal to solutions $\mathbf{c}^*$ of the homogeneous adjoint equation

$$\mathcal{L}^*\mathbf{c}^* = \mathbf{0}. \tag{2.47}$$

The only solutions of the adjoint problem (with appropriate boundary conditions) have spatial dependence $\mathbf{c}^* = \mathbf{b}\cos(k_f x)$. Here we may employ the trigonometric identity $2\cos^2\theta = \cos 2\theta + 1$ to show that, under an appropriately defined inner product, $\mathcal{Q}_2$ is always orthogonal to $\mathbf{c}^*$. Hence, from the solution of the homogeneous equation, (u_2, v_2) will be determined only up to the addition of constant multiples of u_1 and v_1 respectively.

On substitution of the expressions for $\mathbf{c}_1$ and $\mathbf{c}_2$ into (2.42) for the linear equation (2.38) with $n = 3$, we arrive at the $\mathcal{O}(\epsilon^3)$ equation. On application of the Fredholm

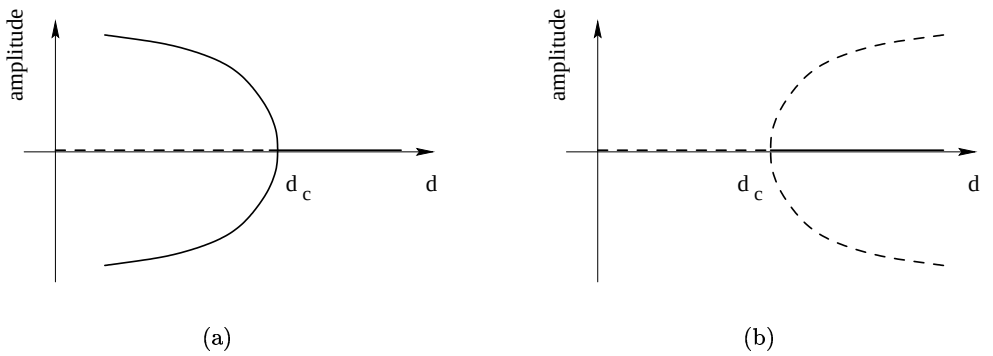

FIGURE 2.3 Schematic bifurcation diagrams for the pitchfork bifurcation (2.49) showing (a) supercritical and (b) subcritical bifurcations. Solid lines represent stable solutions and dotted lines unstable solution branches.

Alternative Theorem we find that the null vector of the adjoint $\mathbf{c}^*$ is no longer automatically orthogonal to $\mathcal{Q}_3$. We require orthogonality for solutions of the $\mathcal{O}(\epsilon^3)$ problem, giving a *solvability condition* by which secular terms (those with spatial dependence $\cos(k_f x)$) in $\mathcal{Q}_3$ are suppressed. The structure of this condition leads to an equation for the amplitude $a(\tau)$ of the form

$$\frac{da}{d\tau} = P_1\, a(\tau) + P_3\, a^3(\tau). \tag{2.48}$$

2.4.2 Amplitude Equation. Equation (2.48) is the *amplitude equation* for the pitchfork bifurcation. The absence of quadratic terms is due to symmetries in the spatial freedom of the system (see Nicolis [93]) and ensures that the two nontrivial steady state solutions are symmetric, corresponding to the two polarities identified for the linear problem. Writing in terms of the physical parameters, $\epsilon = \sqrt{d_c - d}$ and time $t = \tau/\epsilon^2$, the rescaled amplitude $z(t) = \epsilon a(t)$ satisfies

$$\frac{dz}{dt} = (d_c - d)\, P_1\, z(t) + P_3\, z^3(t) \tag{2.49}$$

with three fixed points

$$z_0 = 0 \tag{2.50}$$

$$z_\pm = \pm\sqrt{(d - d_c)\,\frac{P_1}{P_3}} \tag{2.51}$$

the first of which is identified with the homogeneous steady state of the reaction-diffusion equation. The stability of the branches is easily deduced from a linear stability analysis of the amplitude equation. The homogeneous steady state z_0 is stable for $d > d_c$ when $P_1 > 0$, which must therefore be the case for the Turing bifurcation. Then if $P_3 < 0$, solutions $z_\pm$ exist and are stable for $d < d_c$, giving a supercritical bifurcation as shown schematically in Figure 2.3(a), while for $P_3 > 0$ solutions $z_\pm$ exist for $d > d_c$ and are unstable, the subcritical case, shown in Figure 2.3(b). All of the

kinetic systems that are studied in this thesis give rise to supercritical bifurcations.

The asymptotic approximation to the long-time steady heterogeneous solution of the reaction-diffusion equation is given by

$$\mathbf{c}(x) = \begin{pmatrix} u(x) \\ v(x) \end{pmatrix} = \begin{pmatrix} u_s \\ u_s \end{pmatrix} \pm \sqrt{\left|(d_c - d)\frac{P_1}{P_3}\right|} \begin{pmatrix} \bar{u} \\ \bar{v} \end{pmatrix} \cos(k_f x) + \mathcal{O}(d_c - d). \quad (2.52)$$

We may deduce the influence of the scaling parameter γ in the nonlinear analysis without recourse to explicit calculation of P_1 and P_3 and the null vectors for a specific reaction scheme, all of which may depend on γ. One quickly sees that γ appears only in $\mathcal{L}$ and $\mathcal{Q}_3$ and hence will be present in the expression (2.52), and in particular the amplitude $z_\pm$, only as the quotient k_f^2/γ. Therefore γ will have the same influence as described in section 2.3.2 for the linear analysis. The maximum amplitude for all choices of mode k_f as γ is varied will be the same. Thus we expect all primary solution branches to have the same form, appropriately scaled along the γ axis for different k_f, and this is illustrated with concrete numerical examples below. Next we discuss the implications of this symmetry on the pattern modes.

2.4.3 Symmetries of the Steady State Patterns. Steady heterogeneous solutions to the reaction-diffusion equations exhibit a symmetry in the relationship between different primary bifurcation branches, and thus between patterns of different mode. This symmetry will prove to be a useful tool in examining patterns formed on the growing domain, where we show that the arguments may be extended to the full PDE system. To illustrate the symmetry we construct periodic solutions for the steady state equations from solutions of lower mode. To simplify notation we will consider a scalar reaction-diffusion equation, however, the result applies equally well to systems, where heterogeneous patterns form through the Turing instability. Recently this symmetry has also be noticed by Nishiura and Ueyama [95] and has previously been described for the steady state problem by Kevrekidis and Brown [63], who extend the arguments considerably to encompass the prediction of secondary ('mixed-mode') branches.

We consider solutions to the steady state problem

$$0 = \frac{1}{\gamma}\frac{\mathrm{d}^2 c}{\mathrm{d}x^2} + R(c), \quad x \in [0,1] \quad (2.53)$$

where $\gamma = \omega L^2/D$, with zero flux boundary conditions

$$\frac{\mathrm{d}c}{\mathrm{d}x} = 0, \quad x = 0, 1. \quad (2.54)$$

Let us suppose that for $\gamma = \gamma_1 > \gamma_c$ the solution consists of the primary mode m, where the linearised equations have solution with heterogeneity $\cos(m\pi x)$. We can construct new solutions by scaling, translating and reflecting this pattern. To obtain

a new pattern, $q_{2m}(x)$, of mode $2m$ we use the tent map transformation

$$p_2(x) = \begin{cases} 2x, & 0 \le x < \frac{1}{2} \\ 2\,(1-x)\,, & \frac{1}{2} \le x \le 1 \end{cases} \tag{2.55}$$

such that

$$q_2(x;\gamma_1) \equiv c(p_2(x);\gamma_1), \tag{2.56}$$

which satisfies the equation

$$0 = \frac{1}{4\gamma_1}\frac{\mathrm{d}^2 q_2}{\mathrm{d}x^2} + R(q_2). \tag{2.57}$$

The transformation $p_2(x)$ ensures that the zero flux conditions are satisfied at the boundaries of the unit interval, and so $q_2(x;\gamma)$ is a solution of the *same* equation as $c(x;\gamma_1)$ when $\gamma = 4\gamma_1$, i.e. when the domain length is doubled. The transformation has discontinuous derivative at the point $x = 1/2$, however, $q_2(x)$ has zero gradient here by construction and is, therefore, twice continuously differentiable. Patterns constructed under the transformation $p_2(x)$ from odd modes maintain the same polarity as the original pattern mode. Just as easily, patterns with the opposite polarity are constructed by the complementary transformation

$$\overline{p}_2(x) = \begin{cases} 1-2x, & 0 \le x < \frac{1}{2} \\ 2x-1, & \frac{1}{2} \le x \le 1 \end{cases} . \tag{2.58}$$

It is straightforward to see that a general transformation $p_m(x)$ can be defined in a similar manner to generate a pattern of mode m on the interval $[0,1]$ from the first mode $m = 1$, and to find the corresponding equation. In general $q_m(x;\gamma) \equiv c(p_m(x);\gamma)$ satisfies the same equation as $c(x;\gamma_1)$ when $\gamma = m^2\gamma_1$, or otherwise, when the domain length increases by a factor m. This explains the structure of Figure 2.2, where linear growth rates for different mode are simply scaled along the γ axis, and is similarly reflected in Figure 2.1 where the intersections of instability line up for modes related by these transformations.

2.5 Pattern Selection

As the control parameter, for example d or γ, is moved further past the bifurcation point, d_c or γ_c, an increasing range of solutions to the linear problem are admissible as growing linear modes. Furthermore, ranges of instability of the homogeneous steady state to different modes overlap increasingly as the system moves further from the critical point (see Figure 2.1 for the effect of decreasing d on the intervals in γ). The effect on pattern selection is illustrated in Figure 2.4. The conspicuous curves, which comprise sets of points from individual numerical simulations, represent steady state patterns of the same mode (we do not distinguish between the two polarities), with amplitude changing as γ increases. We draw attention to several notable features. Firstly, as predicted by linear and nonlinear analysis alike, the maximal amplitude

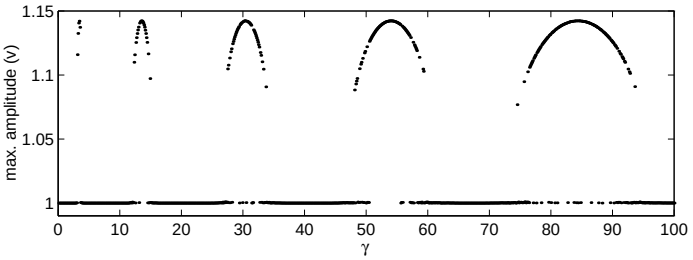

(a)

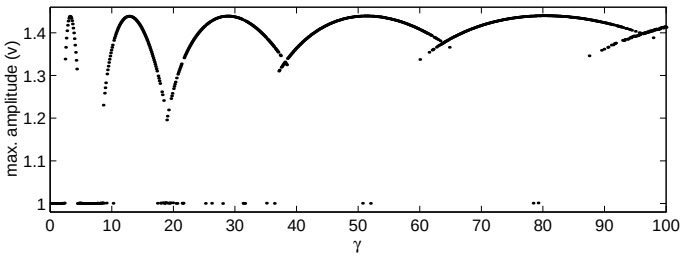

(b)

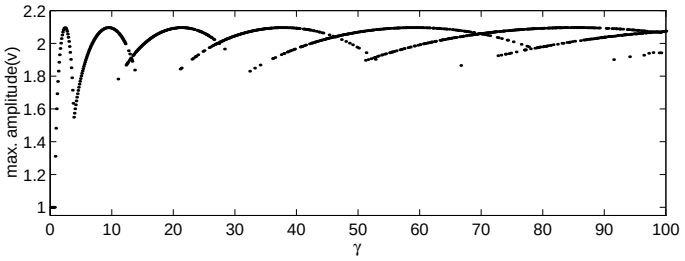

(c)

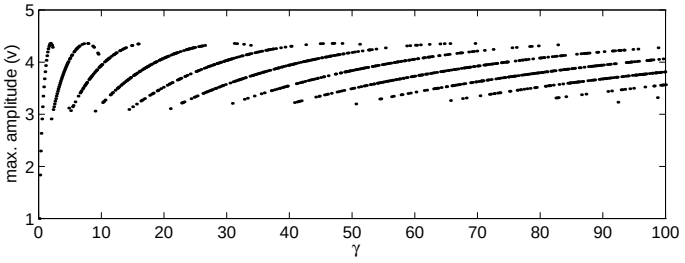

(d)

FIGURE 2.4 The disappearance of intervals of stability in γ and increase of multiplicity of solutions as d is decreased ($\epsilon = \sqrt{d_c - d}$ is increased), where (a) $d = 0.115$ ($\epsilon \approx 0.045$), (b) $d = 0.1$ ($\epsilon \approx 0.13$), (c) $d = 0.05$ ($\epsilon \approx 0.26$) and (d) $d = 0.01$ ($\epsilon \approx 0.38$). Each point shows the final steady amplitude for the activator v on a domain of fixed size, where the value of the scaling parameter γ is held constant during numerical simulation (the homogeneous steady state has amplitude $v = 1$). The initial conditions for each data point consist of random perturbations around the homogeneous steady state, of amplitude 1%. We have used Schnakenberg kinetics with $a = 0.1$, $b = 0.9$.

(as γ varies) for each mode is the same, independent of the wavenumber. Indeed the simple scaling of the branches for different modes can be discerned, illustrating the symmetry that we have described.

Close to the bifurcation point (when ϵ is smallest, in Figure 2.4(a)) there are intervals of stability of the homogeneous steady state between regions where a finite amplitude pattern is realised. These intervals rapidly disappear as d is decreased and are replaced by increasing overlap of solution branches. Where overlap occurs in the figure, two or more different steady solutions have been generated for domains of (approximately) the same size, but from different initial data. Here, in the competition between different growing modes, the initial data dominates the pattern selection (through the components of $\mathbf{y}_m$ in the linear analysis), rather than the linear growth rate. This dependence on the initial conditions clearly increases as d recedes from its critical value. In the nonlinear regime, competition between modes may be described using amplitude equations, as derived in the previous section. This approach is particularly appropriate for investigating the nonlinear interactions between modes in two-dimensional (and higher) spatially-distributed systems, where the selection between patterns of different planforms may be predicted. This is discussed further in Chapter 6.

2.5.1 Multiplicity of Solutions: the Robustness Problem. The distribution of steady patterns achieved for different sets of initial conditions on domains of fixed size, corresponding to fixed values of γ, is shown in Figure 2.5. From the dispersion relation we have calculated the value of γ for which different modes achieve maximum linear growth rate, calling these modes $m_\star$. We have performed repeated numerical simulations with these values of γ for different sets of random initial data and compiled tables of the relative frequency of occurrence of different steady pattern modes for two values of d, namely $d = 0.05$ in Figure 2.5(a) and $d = 0.01$ in Figure 2.5(b). Thus for (b) the distributions show the relative frequencies for the different solution branches found in Figure 2.4(d), at three different values of γ (and similarly (a) corresponds to Figure 2.4(c)). Two results are immediately apparent: firstly, the mean of the distributions tends towards lower modes than the linearly predicted fastest growing mode $m_\star$, becoming progressively lower for larger γ, and secondly the width of the distribution is smaller for d nearer d_c and increases with γ. Thus for different sets of initial data an increasingly wide range of pattern modes my be generated as the domain length increases. Put otherwise, for larger domain lengths the initial conditions must be controlled with increasing sensitivity to reliably pick out one particular mode.

This encapsulates the *robustness* problem for reaction-diffusion pattern formation. In order to generate patterns reliably, conditions such as the initial data and the size of the domain must be closely controlled. This has been a major source of criticism of the application of reaction-diffusion models to those biological situations in which a specific number of pattern units (spatial oscillations) must be reliably produced.

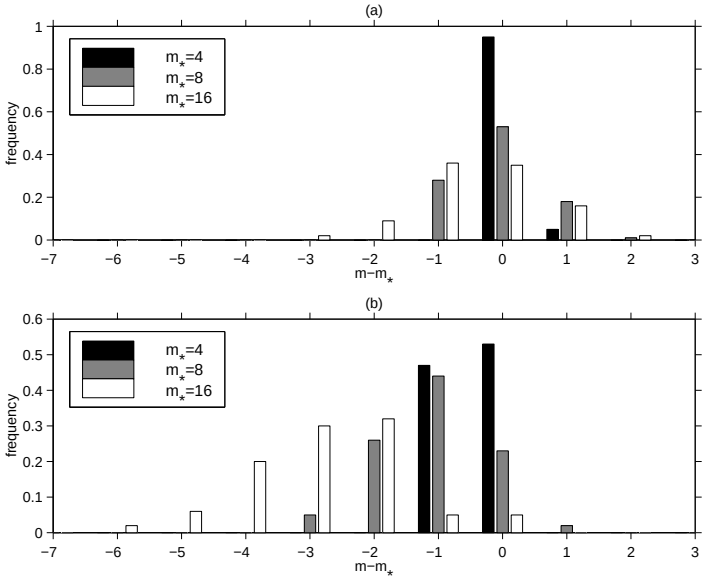

FIGURE 2.5 Relative frequency of occurrence of different modes m on domains of various fixed sizes from random initial data. Each figure shows frequency distributions corresponding to three values of γ, each chosen so that a particular mode $m_\star$ has maximal linear growth rate. These values of γ, calculated from the dispersion relation (for Schnakenberg kinetics), depend on d. In each case we plot the relative frequency (from a sample of 100) against $m - m_\star$, the distance in mode number of the steady pattern generated, m, from the linear prediction, $m_\star$. For (a) $d = 0.05$ and we take $\gamma = 33.4$ (black) where $m_\star = 4$ has fastest linear growth rate, $\gamma = 133.4$ (grey) for which $m_\star = 8$ is fastest growing and $\gamma = 533.4$ (white) for $m_\star = 16$. In (b) $d = 0.01$ and the values of γ are 13.3, 53.2 and 212.9 respectively. We note that the two pattern polarities were observed in roughly equal numbers (data not presented).

The problem is further compounded in higher spatial dimensions where the domain geometry must also be sensitively controlled, and where many more pattern modes tend to be admissible for any particular domain size and geometry.

2.5.2 Mechanisms of Pattern Selection. For equilibrium systems the pattern selection problem is solved by minimising a free energy functional and, at least in principle, solutions evolve towards the lowest energy state. No such general method is available for nonequilibrium systems. We have considered the role of domain size (and geometry) and of the initial data, which might be deemed *static* effectors of pattern selection. A full discussion and examples from other pattern forming instabilities is presented in the review article by Cross and Hohenberg [21]. Arcuri and Murray [3] report on a study of the influence of boundary conditions on the sensitivity of heterogeneous pattern to various initial conditions. Dillon *et al.* [26] investigate mixed scalar boundary conditions on a one-dimensional domain, and find that Dirichlet conditions for one but not both species at the boundaries reduces the sensitivity on domain scale and initial conditions. In general the boundaries are of greater importance in systems

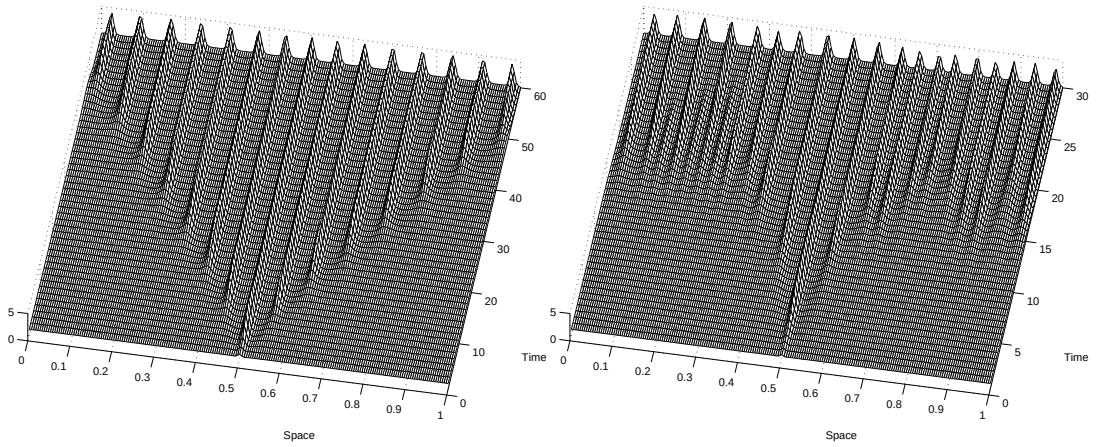

(a) (b)

FIGURE 2.6 Pattern selection behind a travelling front, initiated in the centre of the domain with (a) homogeneous conditions elsewhere and (b) random noise on the domain, $v_0(x) = \big(1+0.01\eta(x)\big)v_s$ where $\eta(x) \in [-1,1]$ is a random variable. For these simulations we use Schnakenberg kinetics with $a = 0.1$, $b = 0.9$, $d = 0.01$ and $\gamma = 1600$.

of small spatial extent and zero flux conditions are found to have the weakest influence on pattern selection.

Similarly there are *dynamic* processes which may determine the final steady pattern. For parameters that vary with time the trajectory taken through parameter space may contribute to pattern selection. For small variations in parameters the solution may be expected to adiabatically follow a stable solution branch of the steady state problem. Where the parameter variation is sufficiently great that the solution moves between solution branches the manner of transitions between the branches becomes important. The bifurcation structure will determine whether or not there is a continuous adiabatic connection between stable branches. These ideas are discussed below in light of results for pattern formation on growing domains.

Murray [88] suggests that the mechanism of initiation of pattern formation on the domain may determine the mode selected. From an initial disturbance at some location on an otherwise homogeneous domain, spatially periodic pattern spreads out to fill the domain behind a 'travelling wave of initiation'. This is demonstrated in Figure 2.6(a). The wavelength of the pattern may be calculated and lies within the linearly destabilising band. If the domain is bounded (and especially if the domain is small) then boundary effects will also affect the final wavelength, as the pattern relaxes to accommodate the conditions imposed there. However, this selection mechanism relies on the initial perturbation being restricted to some small region, and for even a low level of random noise elsewhere on the domain the wavelength of the final pattern cannot be reliably predicted, as demonstrated in Figure 2.6(b).

2.5.3 Reflection and Splitting of Travelling Pulses in the Gray-Scott Model. In general, reaction-diffusion systems can display a rich variety of spatio-temporal phenomena in response to *large amplitude* perturbations. The nature of the kinetic terms plays the major role in determining the solution behaviour. In this thesis we will consider only kinetic schemes which have a single steady state, such that $\mathbf{c}_s$ is the unique solution of $\mathbf{R}(\mathbf{c}_s, p) = \mathbf{0}$. However, for bistable systems an additional pair of solutions, one stable and the other linearly unstable, appear in a saddle-node bifurcation as some kinetic parameter varies. The Gray-Scott model [45] (see Appendix A.2) is an example of a kinetic scheme which, for suitably chosen parameters, demonstrates bistability, and has been extensively studied. In the vicinity of the bistable regime, several interesting spatio-temporal phenomena have been reported. Pearson [109] first identified self-replication of spot-like patterns in two-dimensional numerical simulations of the Gray-Scott model, amongst various other behaviours, some exhibiting spatio-temporal chaos (typically from the interaction of Turing and Hopf modes). This behaviour was observed for sufficiently large perturbation away from the trivial homogeneous steady state, and in a parameter regime in the vicinity of both a Hopf bifurcation in the kinetics, and a subcritical Turing bifurcation for the nontrivial steady state. Many of the patterns reported by Pearson had previously or were subsequently identified in chemical experiments on the FIS reaction by Lee, Swinney and co-workers [70, 71] (reviewed in [72]).

Corresponding phenomena in one-dimensional systems have been studied numerically by Petrov *et al.* [112], Reynolds *et al.* [115] and Rasmussen *et al.* [114]. Depending on the precise location in parameter space (while remaining in the vicinity of the curve bounding the bistable region) these authors have reported that finite initial perturbations may produce various behaviours. Travelling pulses which are reflected from zero flux boundaries are found in a region for which there is a unique steady state, reproduced in Figure 2.7(a). Also it is found that these pulses are reflected during collisions with other pulses [112]. Wave splitting (or self-replication of pulses), illustrated in Figure 2.7(b), is observed for small enough d in the bistable region and, for parameters for which there is a single stable branch, in the vicinity of the saddle-node bifurcation. For the latter case Petrov *et al.* have suggested that in this region the kinetics show excitable dynamics, where small perturbations decay exponentially to the globally stable steady state but sufficiently large perturbations result in long excursions through the phase space before returning to the fixed point. During this excursion the system is in a refractory (non-excitable) state (for a discussion see, for example, Murray [88]). They suggest that by decreasing d the wave back becomes decreasingly refractory, until finally it excites a secondary wave which moves off in the opposite direction. However, Nishiura and Ueyama [95] have shown that the splitting phenomena may be recovered for d near unity, by judicious choice of the kinetic parameters.

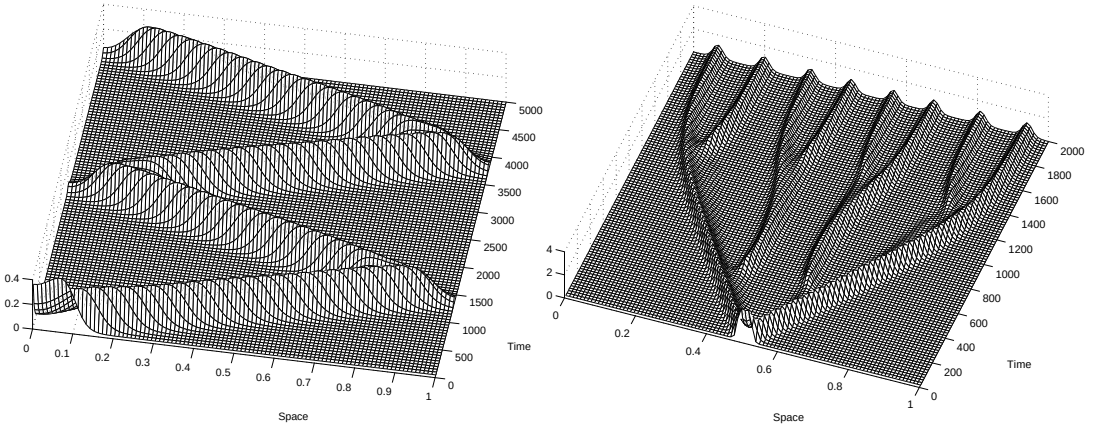

(a) (b)

FIGURE 2.7 Dynamic phenomena in the Gray-Scott model: (a) travelling wave reflection at zero flux boundaries (parameters from [95]), with $F = 0.025$, $k = 0.0544$ (monostable region) and $d = 0.5$ with $\gamma = 12500$. (b) wave-splitting (parameters from [115]) with $F = 0.059$, $k = 0.02$ (bistable region) and $d = 0.01$ with $\gamma = 3600$.

Several authors have investigated the pulse-splitting phenomenon in the Gray-Scott model analytically. Osipov and Severtsev [97] discuss splitting and periodic patterns on infinite domains. Reynolds *et al.* [116] present a heuristic explanation for self-replication of spots and analyse equations of motion for travelling pulses in the limit of small d. Nishiura and Ueyama provide an argument based on underlying 'hidden' symmetries in the bifurcation structure of such reaction-diffusion equations. The authors show that the transient dynamics from the initial perturbation move in the vicinity of saddle-node bifurcations for steady Turing structures, which is reflected in the splitting process observed. Finally we note that although there is no supercritical Turing bifurcation for either solution branch, the transient splitting of travelling pulses may lead to steady Turing-type structures, which appear in a saddle-node bifurcation rather than through DDI, as shown in Figure 2.8(a). However, long-time behaviour may also give oscillating 'mixed mode' behaviour, as in the example shown in Figure 2.8(b). In order to excite these spatio-temporal phenomena a sufficiently strong initial perturbation is required to escape exponential relaxation back to the trivial homogeneous state. Furthermore, these behaviours are restricted to narrow regions of parameter space (in the vicinity of the bistable region) for models such as the Gray-Scott system which have a highly complicated bifurcation structure. As we saw previously (Figure 2.6(a)), large initial perturbations for the simpler Schnakenberg system do not produce pulse splitting. Similar phenomena may, however, be generated for reaction-diffusion equations with Schnakenberg kinetics (and for other comparable systems) when pattern formation is driven by domain growth. In the following chapter we derive the governing equations for reaction and diffusion on a growing domain

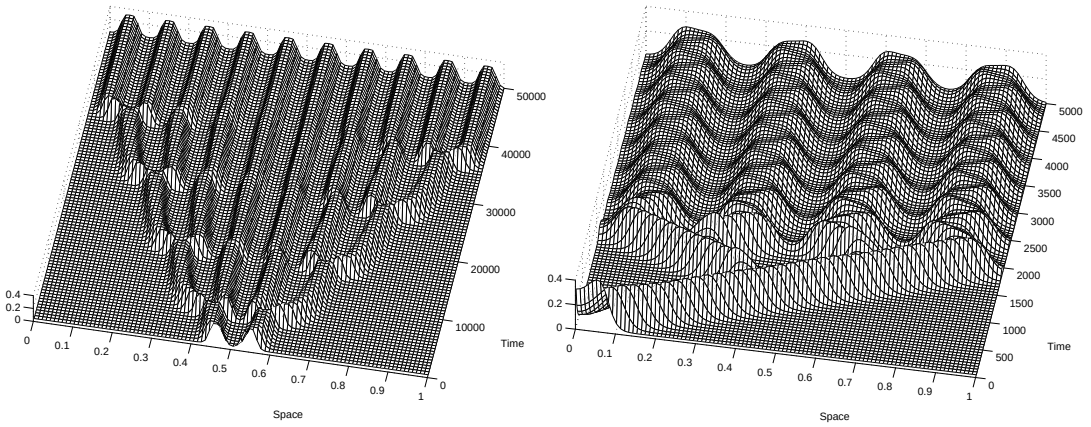

(a) (b)

FIGURE 2.8 Establishment of (a) steady and (b) oscillatory heterogeneous patterns for the Gray-Scott model with (a) $F = 0.04$, $k = 0.06075$ (parameters from [95]) and (b) $F = 0.025$, $k = 0.0542$, for both of which the kinetics have a unique steady state (but are close to the bistable region) and $d = 0.5$. In (a) $\gamma = 2 \times 10^5$ and in (b) $\gamma = 2.5 \times 10^4$.

and in the remainder of the thesis we go on to analyse pattern formation subject to underlying domain growth.